HOKKAIDO UNIVERSITY

Title	Dissecting the role of SMN multimerization in its dissociation from the Cajal body using harmine as a tool compound
Author(s)	Ohazama, Saki; Fujimoto, Akiko; Konda, Daisuke et al.
Citation	Journal of Cell Science, 137(18), jcs261834 https://doi.org/10.1242/jcs.261834
Issue Date	2024-09-30
Doc URL	https://hdl.handle.net/2115/96202
Type	journal article
File Information	jcs261834.pdf

Hokkaido University Collection of Scholarly and Academic Papers : HUSCAP

© 2024. Published by The Company of Biologists Ltd | Journal of Cell Science (2024) 137, jcs261834. doi:10.1242/jcs.261834

RESEARCH ARTICLE

Dissecting the role of SMN multimerization in its dissociation from the Cajal body using harmine as a tool compound

Saki Ohazama[1], Akiko Fujimoto[2], Daisuke Konda[1], Ryota Yokoyama[2], Shinichi Nakagawa[1,2] and Hiroshi Maita[1,2,*]

ABSTRACT

Survival motor neuron protein (SMN), which is linked to spinal muscular atrophy, is a key component of the Gemin complex, which is essential for the assembly of small nuclear RNA-protein complexes (snRNPs). After initial snRNP assembly in the cytoplasm, both snRNPs and SMN migrate to the nucleus and associate with Cajal bodies, where final snRNP maturation occurs. It is assumed that SMN must be free from the Cajal bodies for continuous snRNP biogenesis. Previous observation of the SMN granules docked in the Cajal bodies suggests the existence of a separation mechanism. However, the precise processes that regulate the spatial separation of SMN complexes from Cajal bodies remain unclear. Here, we have employed a super-resolution microscope alongside the β-carboline alkaloid harmine, which disrupts the Cajal body in a reversible manner. Upon removal of harmine, SMN and Coilin first appear as small interconnected condensates. The SMN condensates mature into spheroidal structures encircled by Coilin, eventually segregating into distinct condensates. Expression of a multimerization-deficient SMN mutant leads to enlarged, atypical Cajal bodies in which SMN is unable to segregate into separate condensates. These findings underscore the importance of multimerization in facilitating the segregation of SMN from Coilin within Cajal bodies.

KEY WORDS: Super-resolution microscopy, Cajal body, SMN, Coilin, Harmine

INTRODUCTION

Recent studies have illuminated the assembly mechanisms of membraneless organelles (MLOs), which are primarily assembled by multivalent interactions involving the intrinsically disordered regions of their constituent molecules, as well as RNAs (Borcherds et al., 2021; Hirose et al., 2022; Uversky, 2017). Although many MLO components dynamically shuttle across the boundary of their molecular condensate, the molecular mechanisms determining how specific components are released from MLOs, while others remain inside, have yet to be clarified. Spliceosomal small nuclear RNA-protein complexes (snRNPs) undergo a unique maturation pathway. After transcription in the nucleus, small nuclear RNAs (snRNAs) are exported to the cytoplasm where they acquire a 5′ cap hyper-methylation, associate with Sm proteins and then re-enter the nucleus for further modifications (Meier, 2017; Staněk, 2017). The survival motor neuron protein (SMN), an essential component of the Gemin complex, is pivotal for the early assembly of snRNPs in the cytoplasm and facilitates the nuclear transport of partially matured snRNPs (Paushkin et al., 2002; Pellizzoni et al., 1998). Upon nuclear translocation, both SMN and snRNPs predominantly localize to Cajal bodies, which are nuclear MLOs enriched with factors that mediate the final maturation of snRNPs (Matera, 1998; Staněk, 2017).

In these bodies, SMN associates with multiple components, particularly Coilin, a structural element of Cajal bodies. Their interaction is mediated by the interaction between the symmetrically di-methylated arginine (sDMA) residue on Coilin and the Tudor domain of SMN (Courchaine et al., 2021; Hebert et al., 2001; Tapia et al., 2014). Intriguingly, SMN and Coilin do not randomly intermingle within Cajal bodies; instead, they form distinct molecular condensates described as a ‘ball-in-socket’ structure when visualized using super-resolution microscopy (Courchaine et al., 2021). For continuous snRNP biogenesis in interphase cells, an efficient recycling mechanism for SMN from Cajal bodies is indispensable (Morris, 2008). However, the mechanism of SMN egress from Cajal bodies remains unclear. Notably, the Gem, another nuclear MLO that contains the SMN-Gemin complex but lacks Coilin and snRNPs, is often detected adjacent to Cajal bodies in specific cell types (Liu and Dreyfuss, 1996). Owing to its molecular composition, the Gem is proposed to function as an intermediary site for SMN recycling after its departure from the Cajal body (Morris, 2008), although definitive evidence for this theory remains elusive.

In this study, we used structured illumination microscopy (SIM) to re-examine the internal fine structures of Cajal bodies. Consistent with previous findings, we observed that SMN forms spheroidal condensates enveloped by Coilin, resulting in a distinctive cylindrical structure (Courchaine et al., 2021). Interestingly, we identified a diverse array of Cajal body variants, each displaying different distributions of SMN and Coilin. This suggests that Cajal bodies dynamically alter their shape and composition. Using harmine as a tool compound to transiently disrupt Cajal bodies, we observed that the structural diversity of Cajal bodies is correlated with the maturation of this nuclear MLO. Moreover, the exogenous expression of a multimerization-defective SMN mutant led to the emergence of enlarged Cajal bodies, and the mutant molecule failed to segregate from the nuclear puncta labeled with Coilin. These observations suggest that the multimerization of SMN plays a key role in facilitating the release of SMN from Cajal bodies.

RESULTS

Varied distribution of SMN and Coilin in Cajal bodies

To investigate the cellular processes involved in separating SMN from Cajal bodies, we examined fine distribution of Coilin

[1]Graduate School of Life Science, Hokkaido University, Sapporo 060-0812, Japan. [2]Faculty of Pharmaceutical Sciences, Hokkaido University, Sapporo 060-0812, Japan.

*Author for correspondence (maimai@pharm.hokudai.ac.jp)

S.N., 0000-0002-6806-7493; H.M., 0000-0002-9620-4651

Handling Editor: Megan King
Received 24 November 2023; Accepted 30 August 2024

Journal of Cell Science

and SMN using SIM, a method previously used to reveal fine structures of nuclear body paraspeckles. As previously reported by Neugebauer and colleagues as 'a ball-in-socket configuration' (Courchaine et al., 2021), SMN and Coilin were observed as attached spheres of the separated puncta within Cajal bodies in our analysis using super-resolution microscopy (Fig. 1). However, there are several patterns in their distribution. In smaller Cajal bodies, SMN was observed as a granule that tended to be overlapped or attached with Coilin. On the other hand, in larger Cajal bodies, SMN was often observed in a ring-like shape, as reported previously (Novotný et al., 2015), suggesting a spatially ordered distribution. The sizes of Cajal bodies detected by both Coilin and SMN staining are indicated in the plot with the categorization of each Cajal body (Fig. 1B). This ring-like configuration of SMN was consistent across different antibodies, although the shape of the ring was rougher when using another antibody, clone 2B1; this may be caused by a difference in epitope (Fig. S1A-C). When Coilin formed similar puncta separated from SMN, the Coilin antibody stained the entire area of the puncta. It should be noted that in Cajal bodies in which Coilin completely overlaps SMN as a ring-like structure, the Coilin antibody also stains the structure similarly to the SMN antibody, suggesting that the unstained central region of the ring-like structure somehow prevents access of the antibody. However, this happens only when SMN shows such a ring-like structure, which means that this structure is caused by SMN. In addition, Cajal bodies in other cell lines such as HCT116, HepG2 and U2OS were also observed under the same condition. However, the segregated bodies of Coilin and SMN, which are a characteristic feature of Cajal bodies in our HeLa cells, were not observed in these cells (Fig. S1D). The sizes of Cajal bodies and protein expression levels in these cell lines are comparable with those in HeLa cells, suggesting that the separation of SMN and Coilin in Cajal bodies may require some cell type-specific conditions.

We also observed the location of snRNA within Cajal bodies compared with SMN or Coilin (Fig. 1C,D). Although SMN is thought to be transported to Cajal bodies with snRNPs, U2 snRNA was positioned separately from the SMN cluster when the fluorescence *in situ* hybridization (FISH) signal was detected within Cajal bodies. In contrast, when the U2 signal was detected as a puncta, Coilin was always detected to be overlapping with U2 snRNA. Similar patterns were also observed for small Cajal body-specific RNAs (scaRNAs; data not shown). The co-occurrence of U2 snRNA and scaRNA in a substructure with Coilin is consistent with the function of Cajal bodies in snRNA maturation. These observations of varied positions of sub-structures within Cajal bodies may reflect the steps in the maturation or recycling pathway for SMN. However, the order of the appearance of these different patterns was unclear.

Identification of harmine as a compound that induces Coilin translocation to the peri-nucleolar compartment while SMN persists as granules

We have previously conducted a chemical library screening based on a split luciferase assay and we identified multiple compounds that can regulate cellular U5 snRNP levels (Sato et al., 2023). We were interested in testing whether these compounds may affect the formation of Cajal bodies. Notably, among these compounds, harmine was observed to induce the relocation of Coilin, a major component and common marker of the Cajal body. We found that a compound registered as a harmine derivative induced a localization change of Coilin. However, the compound was unstable, and the actual active compound was harmine, which was yielded by the degradation of the original compound. Therefore, we focused on harmine and observed that harmine induced the relocation of Coilin from the Cajal body to the peri-nucleolar compartment (PNC) (Fig. 2A). We also evaluated three other harmine analogs; however, they were less potent than harmine (Fig. 2A). Only harmol showed some activity, albeit to a lesser extent, in inducing PNC translocation of Coilin. Harmine is known for inhibiting three distinct enzymes: monoamine oxidase (MAOA) (Kim et al., 1997; Rommelspacher et al., 1994), DYRK1A (Bain et al., 2007; Göckler et al., 2009; Wang et al., 2015) and topoisomerase I (TOP1) (Cao et al., 2005; Sobhani et al., 2002). Harmane and harmaline showed negligible PNC translocation of Coilin, although they inhibit MAOA, suggesting that MAOA inhibition does not contribute to this effect. Moreover, when we tested the DYRK1A inhibitor INDY (Kii et al., 2016) and the topoisomerase inhibitor camptothecin (CPT) for potential impacts on Coilin localization, we found no significant effect from INDY. In contrast, CPT induced a Coilin relocation to the PNC in the same way as harmine (Fig. 2B).

Intriguingly, under conditions in which harmine induced the PNC translocation of Coilin, SMN continued to form distinct nuclear foci, independently of Coilin (Fig. 2C), similar to the segregation of SMN from Coilin after cold stress or actinomycin D (Liu and Dreyfuss, 1996). Quantitative analysis is also consistent with the separation of SMN and Coilin staining, and the remaining nuclear bodies involving SMN (Fig. 2D-G). A similar SMN-Coilin separation was observed with camptothecin exposure (Fig. 2C). SMN consistently forms a heterodimer with Gemin2 (Liu et al., 1997). After harmine treatment, Gemin2, like SMN, was visible in nuclear foci separate from Coilin (Fig. 3A). In contrast, Nopp140 (also known as NOLC1), a protein typically found in both nucleoli and Cajal bodies (Bohmann et al., 1995), completely coincided with Coilin at the PNC but was clearly separated from SMN foci (Fig. 3B,C). Fibrillarin (FBL), another protein with dual residence in nucleoli and Cajal bodies, appeared within the nucleolus, but its localization showed a more-diffuse, granule-like structure upon harmine treatment. In this condition, the PNC labeled with Coilin was observed on the surface of the nucleolar structure stained with fibrillarin (Fig. 3D). Colocalization with Nopp140 and fibrillarin after harmine exposure at the nucleolar periphery further supports that the structure where Coilin was localized after harmine treatment is the same as the previously reported PNC (Shav-Tal et al., 2005).

In addition, the distribution of snRNA was also examined using a probe for U2 snRNA (Fig. 4). When Coilin was translocated to PNC after harmine treatment, snRNA puncta disappeared, which may indicate the possibility that the harmine treatment blocks transcription of U2 snRNA, although we have not tested this yet. These observations suggest that a harmine-induced structure detected by anti-SMN antibody is similar to Gem, which includes SMN and the Gemin complex, but not Coilin and snRNA (Fig. 4). The protein levels of Coilin and SMN after harmine treatment were assessed by western blotting and no changes in protein were observed (Fig. S2A).

The harmine-induced translocation of Coilin to the PNC is reversible

Next, we examined whether the removal of harmine would allow cells to reconstitute Cajal bodies. As shown in Fig. 5, harmine removal resulted in the rapid disappearance of Coilin from PNC and the reformation of small Cajal bodies within 30 min after removal. This is supported by the recovery of colocalization coefficient values after harmine removal (Fig. 5D). However, a Gem-like structure often persisted after harmine removal without Coilin association (Fig. 5E), suggesting that the Cajal body restoration

Journal of Cell Science (2024) 137, jcs261834. doi:10.1242/jcs.261834

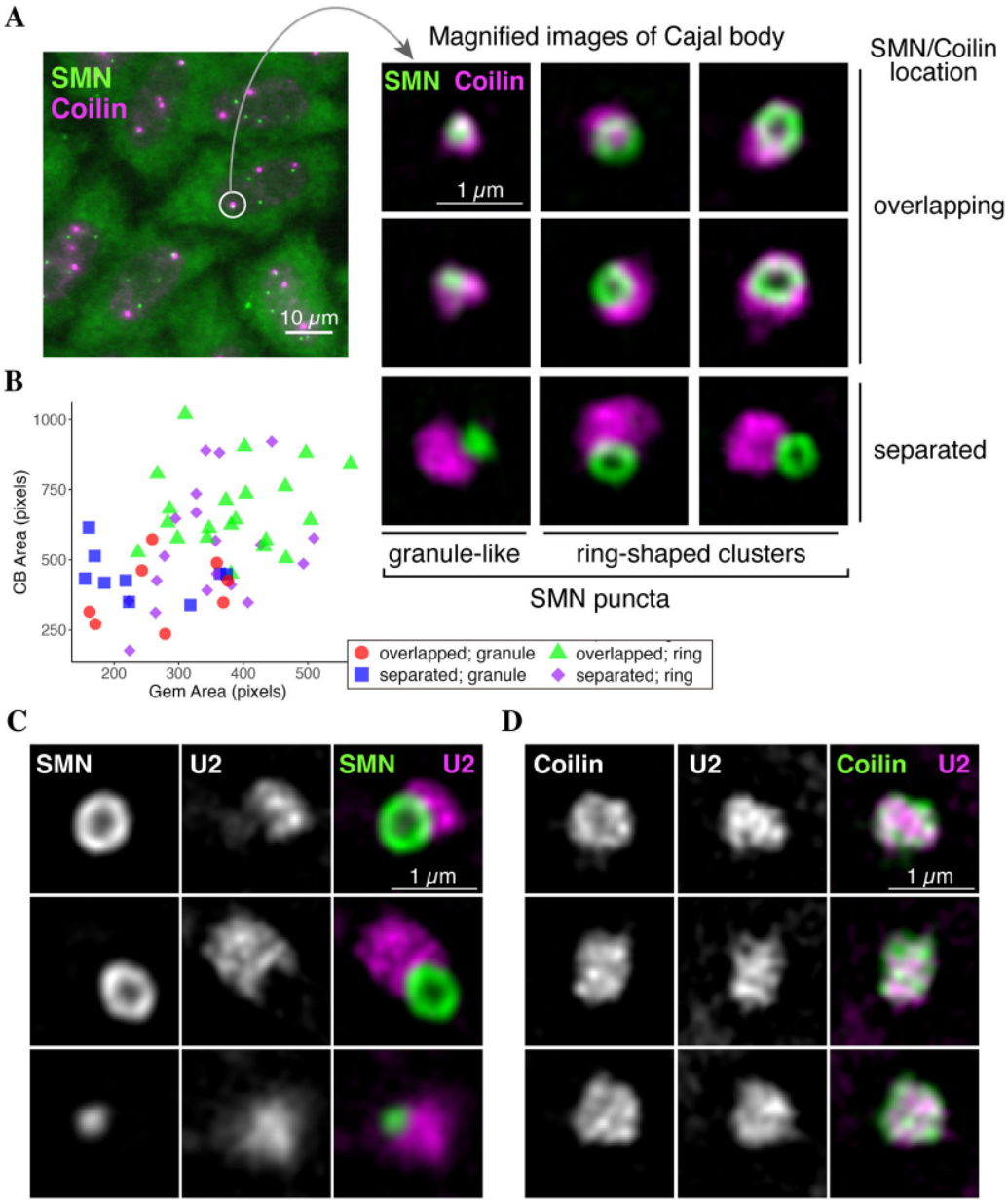

Fig. 1. The fine structure of Cajal bodies, as revealed by SIM, display structural diversity. (A) Cajal bodies and Gems were initially stained using anti-SMN (green) and anti-Coilin (magenta) antibodies (left panel) in HeLa cells. Cajal bodies positive for both antibodies were selected for detailed observation using super-resolution microscopy. SIM images show Cajal bodies stained using anti-SMN (green) and anti-Coilin (magenta) (right panel) antibodies. Depending on the localization of SMN and Coilin puncta, patterns were categorized as 'overlapping' or 'separated', as indicated on the right. SMN puncta were further classified into two types: 'granule-like' or 'ring-shaped clusters', as illustrated below. (B) A plot showing the size of each Cajal body in SIM images, with sizes determined using Coilin and SMN antibodies for Cajal bodies and Gems, respectively. 1 pixel=625 nm^2. Observed Cajal bodies (n=57) are classified into four groups based on their shapes, as indicated in the key. CB, Cajal body. (C,D) SIM images of Cajal bodies where protein components or snRNA were stained using specific antibodies or FISH probes in the following combinations: U2 snRNA and SMN (C), and U2 snRNA and Coilin (D). U2 snRNA puncta were observed to intermingle with Coilin but were only adjacent to SMN. Each experiment was independently repeated at least three times.

does not necessarily use Gem-like structures as a scaffold. Instead, the small Cajal bodies containing both Coilin and SMN at nearly the same size were observed, suggesting that these small Cajal bodies were likely reconstituted *de novo* by the simultaneous assembly of both proteins.

The effect of harmine on Coilin localization was captured by live imaging in HeLa cells transiently expressing Coilin-mRuby2 (see Movies 1 and 2 and snapshots in Fig. 5F). As Coilin rapidly disappears from Cajal bodies after harmine treatment, these puncta may well represent the structures in which Coilin is dynamically exchanged from Cajal bodies (Dundr et al., 2004; Handwerger et al., 2003; Zhu and Brangwynne, 2015). Both Coilin efflux from Cajal bodies and its accumulation in the PNC occurred simultaneously. After harmine washout, the rapid escape of Coilin from the PNC was remarkable, but some residual Coilin protein localized to the tip of the PNC. Residual Coilin often formed larger puncta compared

Journal of Cell Science

Journal of Cell Science (2024) 137, jcs261834. doi:10.1242/jcs.261834

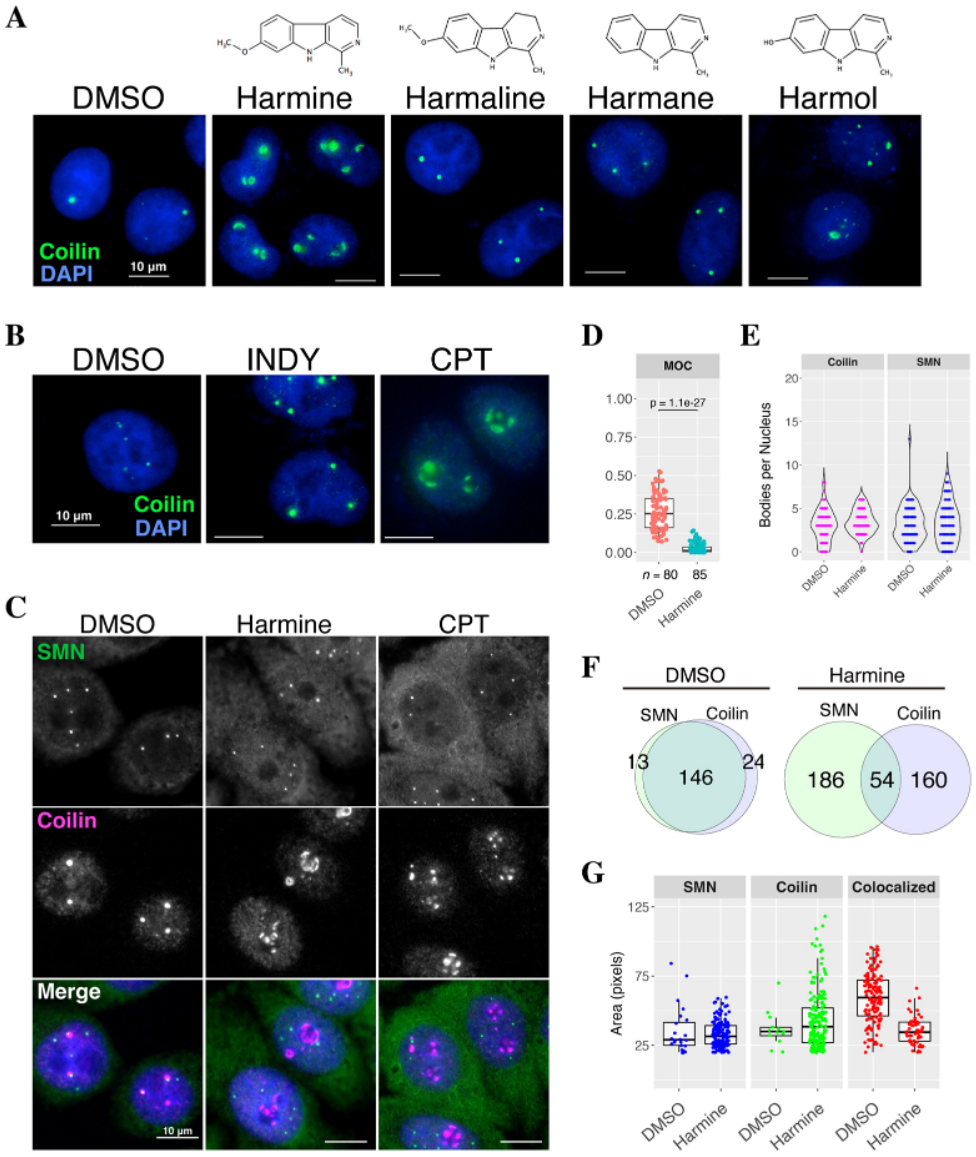

Fig. 2. Harmine induces the translocation of Coilin to the PNC without affecting SMN granules. (A) The localization of Coilin in HeLa cells treated with harmine or its analogs at a concentration of 50 µM for 4 h. The structures of the compounds are indicated above their names. (B) Compounds possessing similar activities to harmine, such as the DYRK1 inhibitor INDY and the topoisomerase I inhibitor CPT, were evaluated for their effects on Coilin localization at concentrations of 20 µM and 25 µM, respectively, for 4 h. Experiments in A and B were independently repeated at least twice. (C) SMN continues to form nuclear granules after harmine exposure. After 3 h of treatment with 50 µM harmine, proteins were stained using specific antibodies targeting SMN and Coilin. This experiment was conducted three times. (D) The colocalization coefficient values (MOC), calculated based on the signal intensity of SMN and Coilin in each nucleus, were compared. The calculated significance values from the Wilcoxon rank-sum test are shown on the plot. (E) A violin plot displaying the number of nuclear dots stained using anti-Coilin or anti-SMN antibodies in each nucleus. (F) Nuclear dots stained for SMN or Colin were counted and classified according to their distance from each other. Dots stained using different antibodies positioned close enough were put into the category of 'colocalization', whereas a dot far from other dots stained using another antibody was labeled 'SMN' or 'Coilin', indicating no colocalization. The number of dots in each category is indicated within the Venn diagram. Colocalization between SMN and Coilin was reduced by harmine treatment. (G) The sizes of each dot are simultaneously plotted using the categories shown in F. 1 pixel=0.01 µm^2. To quantify the puncta, data in D-G are taken from a representative experiment. The box plots in D and G show the median (line), interquartile range (IQR; box), and 1.5 times the IQR from the first and third quartiles (whiskers). DMSO was used as a vehicle control for all treatments.

with the *de novo* assembled Cajal bodies. We observed that SMN was rarely concentrated in this puncta of residual Coilin, whereas Nopp140 colocalized with Coilin (data not shown). This relocation of Coilin between Cajal bodies and the PNC was also observed after the removal of camptothecin, although the recovery was somewhat prolonged compared with harmine (Fig. S3). Conversely, PNC translocation induced by higher concentrations of actinomycin D treatment (Carmo-Fonseca et al., 1992) was rapid but irreversible, possibly owing to severe cell damage (Yung et al., 1990) (Movies 3 and 4; Fig. S4).

SMN progresses to a cluster-like distribution and is associated with the enlargement of newly assembled Cajal bodies

Along with this time course, we used super-resolution microscopy to closely examine the Cajal bodies. After 30 min of recovery

Journal of Cell Science

Journal of Cell Science (2024) 137, jcs261834. doi:10.1242/jcs.261834

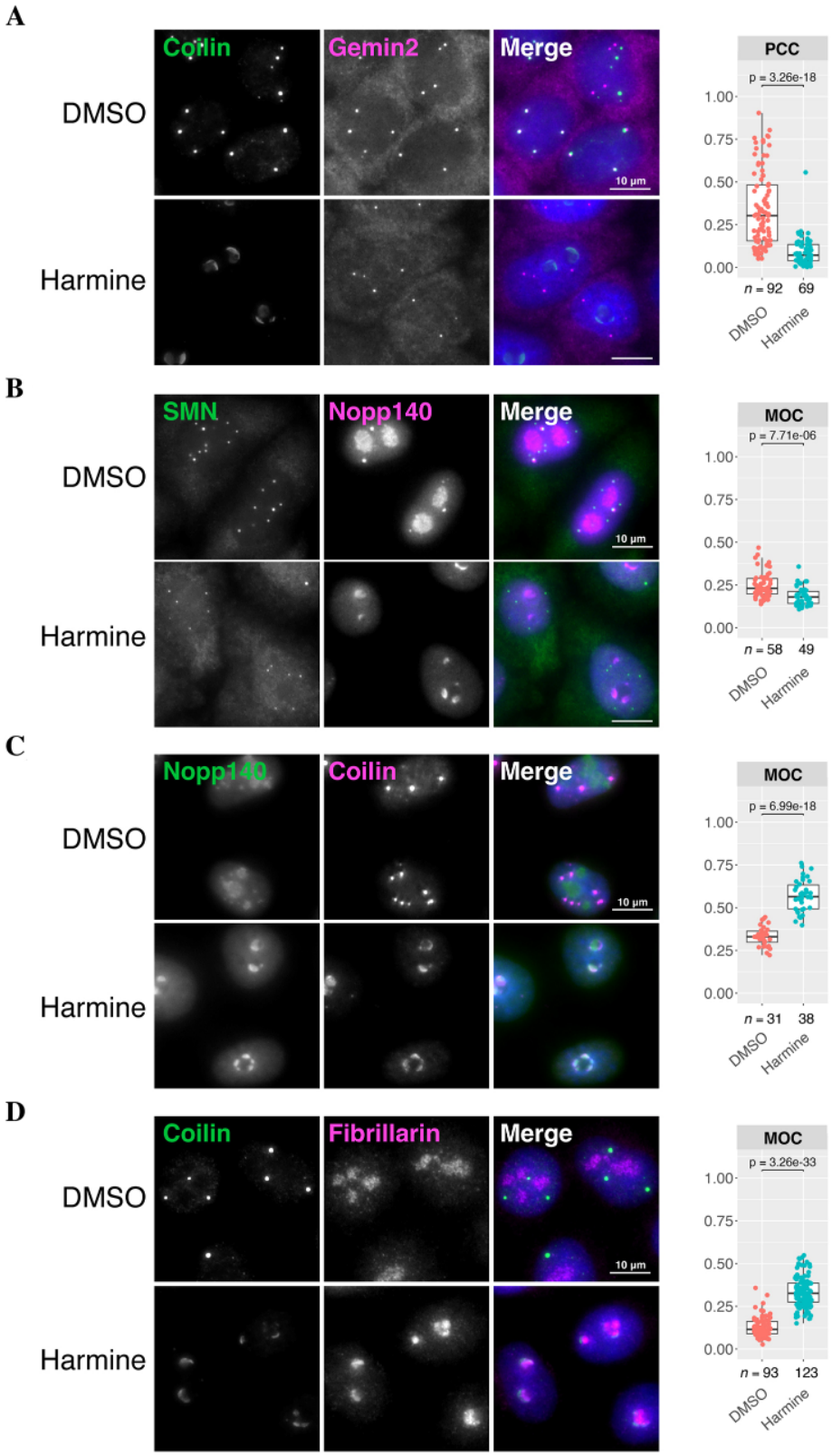

Fig. 3. Colocalization analysis of multiple Cajal body components at both the Cajal body and PNC after harmine exposure. (A-D) In HeLa cells after 3 h of exposure to 50 µM harmine, proteins were stained using specific antibodies in the following combinations: anti-Gemin2 and anti-Coilin (A), anti-SMN and anti-Nopp140 (B), anti-Coilin and anti-Nopp140 (C), and anti-Coilin and anti-fibrillarin (D). SMN and Gemin2 exhibited no harmine-induced relocation to the PNC. Nopp140 and Coilin showed overlapping localization at both the Cajal bodies and the PNC. Fibrillarin also altered its localization upon harmine exposure, but in distinct areas within the nucleolus compared with Coilin. These experiments were independently repeated at least twice. To the right of cell images, a plot shows the colocalization coefficient values for each nucleus, calculated based on the signal intensity of proteins in the left panels. These values were compared between the cells with and without harmine treatment. *n* indicates the number of nuclei used for the plot. The calculated significance values from the Wilcoxon rank-sum test are shown on the plot. The box plots show the median (line), interquartile range (IQR; box), and 1.5 times the IQR from the first and third quartiles (whiskers). DMSO was used as a vehicle control for all treatments.

culture from harmine washout, the small bodies with colocalization of SMN and Coilin, which are assumed to be newly assembled Cajal bodies, were observed as a structure in which the two similar-sized small puncta of SMN and Coilin were attached to each other. After a 120 min recovery period, we observed an increase in larger bodies composed of both SMN and Coilin, and notably SMN puncta often showed a ring-like shape in such structure (Fig. 5C). This suggests that SMN aggregates proceed into more-organized configurations after the restoration of Cajal bodies. It is noteworthy that large SMN ring-shaped structures, which are likely to remain during harmine

Journal of Cell Science

Journal of Cell Science (2024) 137, jcs261834. doi:10.1242/jcs.261834

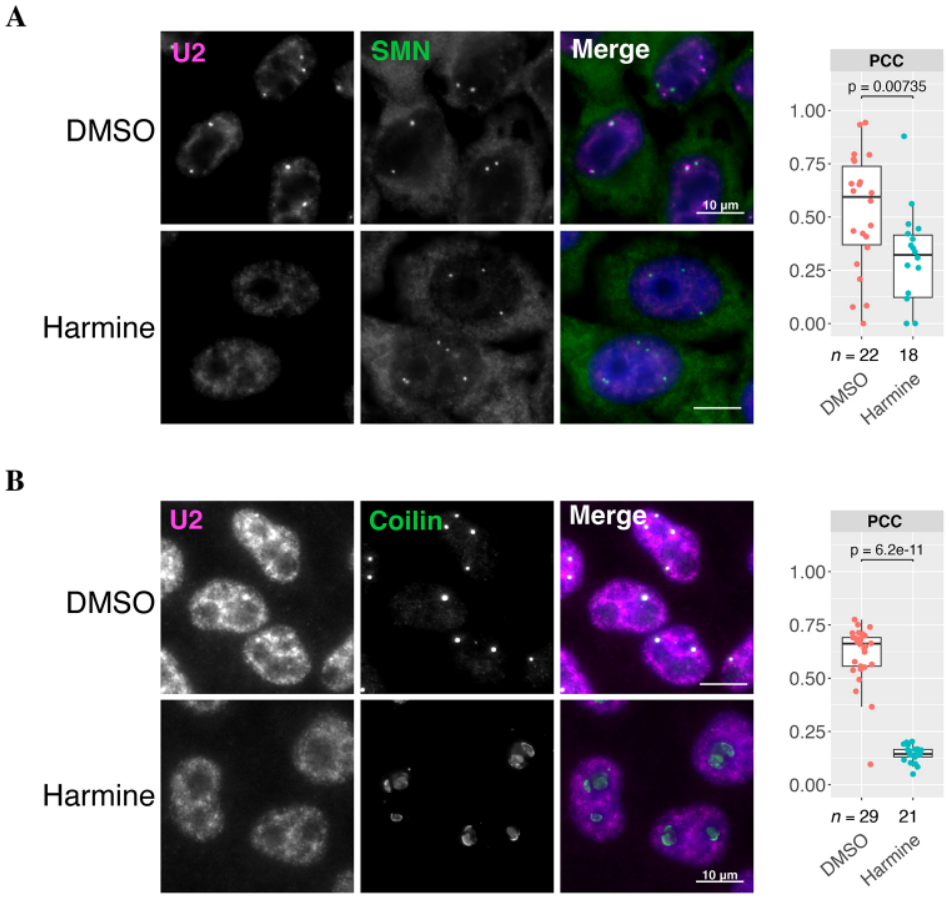

Fig. 4. Colocalization analysis of Cajal body components and U2 snRNA at both Cajal body and PNC after harmine exposure. (A,B) After exposure to harmine for 3 h at 50 µM, Coilin and SMN were double stained using both antibodies and a FISH probe for U2 snRNA in the following combinations: U2 snRNA and SMN (A), and U2 snRNA and Coilin (B). After harmine exposure, U2 snRNA foci at Cajal bodies disappeared, concurrent with Coilin relocation to the PNC. These experiments were independently repeated twice using HeLa cells. To the right of cell images, plots show the colocalization coefficient values for each nucleus, calculated based on the signal intensity of proteins in the left panels. These values were compared between the cells with and without harmine treatment. *n* indicates the number of nuclei used for the plot. The calculated significance values from the Wilcoxon rank-sum test are shown on the plot. The box plots show the median (line), interquartile range (IQR; box), and 1.5 times the IQR from the first and third quartiles (whiskers). DMSO was used as a vehicle control for all treatments.

exposure, still exist after harmine removal, and a small puncta of Coilin is sometimes attached to them. Thus, only some SMN in these remaining bodies may retain the capability to interact with Coilin. Interestingly, FISH signals using a U2 probe were rarely detected in newly formed Cajal bodies, even after 120 min of recovery culture. However, over time, these signals accumulated to form foci of similar size to those before the harmine treatment by 6 h (Fig. S5). This suggests that SMN and Coilin in the nucleus induce the Cajal body formation without the need for freshly imported snRNPs.

Overexpression of either SMN or Coilin causes changes in response to harmine

Aiming to simultaneously monitor SMN and Coilin movements, we transiently transfected the fluorescent-tag fusion Coilin into HeLa cells and confirmed the localization of endogenous SMN. Unexpectedly, overexpression of Coilin recruited SMN to the PNC upon harmine treatment, which was also observed even using small-tag fused Coilin (Fig. S6A). Similarly, overexpression of SMN caused its own translocation to PNC or sequestration of Coilin within Cajal bodies containing SMN in the presence of harmine. Furthermore, when Coilin or SMN was attached to a fluorescent protein, the magnified picture of Cajal bodies obtained by super-resolution microscopy no longer showed Coilin and SMN puncta separated; they appeared mixed within a single structure. However, the observation that the expression of Coilin fused with a V5-tag, which is smaller than a fluorescent protein, did not disturb the distribution suggests that the segregation of SMN from Coilin occurs only when the concentration of both molecules is balanced and these proteins are structurally unconstrained (Fig. S6B).

Colocalization assay using harmine revealed that SMN interacts with Coilin via the Tudor domain

However, we noticed that overexpression of SMN could be used to visualize the interaction with Coilin by monitoring the persistence of their colocalization after harmine treatment. SMA-associated SMN mutations often occur within two protein domains of SMN (Butchbach, 2021): mutants within the Tudor domain, which facilitate condensate formation by binding symmetrically di-methylated arginine in RG repeats of Coilin and Sm proteins (Courchaine et al., 2021), and mutants that impair the function of the C-terminal YG motif, which is essential for SMN multimerization (Martin et al., 2012). Two well-studied mutations, E134 K and Y272C, in each domain were tested for their response to harmine treatment.

As shown in Fig. 6, overexpression of wild-type SMN (SMN WT) induced either PNC translocation of SMN or anchoring of Coilin to Cajal bodies containing SMN after harmine treatment. However, the E134K mutation, a variant associated with SMA that lacks the ability to bind Coilin through the Tudor domain, failed to anchor Coilin to Cajal bodies. Approximately 60% of cells expressing SMN WT showed synchronized recruitment of both SMN and Coilin to the PNC upon harmine treatment, a number that decreased to 25% in cells harboring SMN E134K. We also evaluated another SMA mutant, Y272C, which lacks the multimerizing ability of the C-terminal YG domain. This mutant mirrored the behavior of SMN WT but with a preference for anchoring Coilin to Cajal bodies rather than PNC migration of SMN. The number of such cells increased by ∼1.5-fold (Fig. 6D; Fig. S7).

Journal of Cell Science (2024) 137, jcs261834. doi:10.1242/jcs.261834

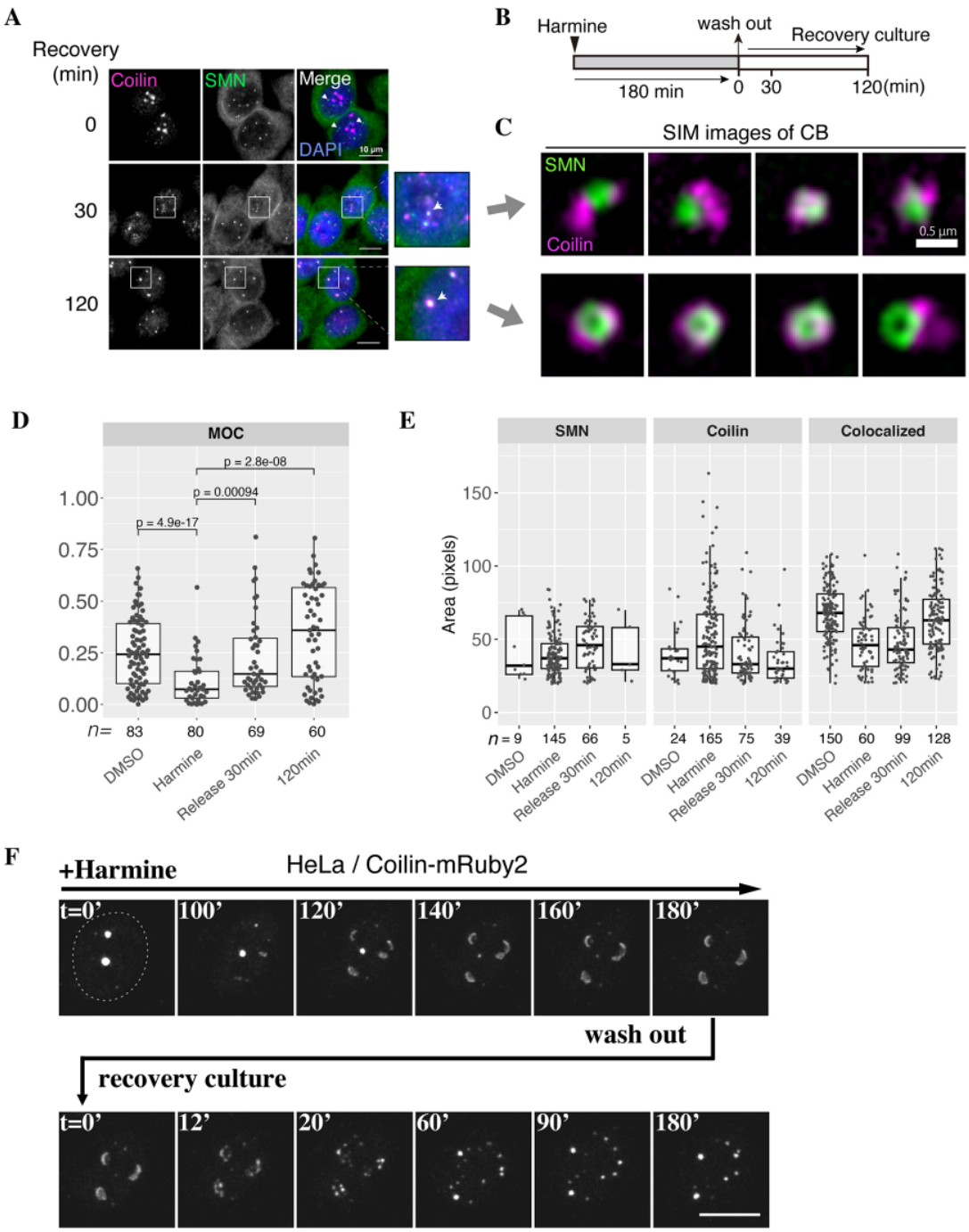

Fig. 5. Coilin rapidly reassembles Cajal bodies upon removal of harmine. (A) Staining of Coilin and SMN at the indicated times of recovery from harmine treatment (as shown in B); boxes indicate regions shown in magnified views, and arrows indicate newly formed Cajal bodies labeled with both Coilin and SMN antibodies. After the washout of harmine, Gem often remained (indicated by arrowheads). These experiments were repeated at least three times. (B) Schematic of the time course for the release experiment using HeLa cells shown in A and C. (C) SIM images of Cajal bodies (CB) after the washout of harmine for the indicated durations from panel A (gray arrows). SMN typically exhibited a granule-like structure after 30 min of recovery culture. However, after 120 min of recovery culture, ring-shaped clusters became more prominent. Experiments were independently repeated twice. (D) The colocalization coefficient values, calculated based on the signal intensity of SMN and Coilin in each nucleus, were compared between harmine treatment and recovery culture conditions. The calculated significance values from the Wilcoxon rank-sum test are shown on the plot. (E) Colocalization of nuclear dots stained with SMN or Colin was evaluated based on their distance from each other, and the sizes of each dot were simultaneously plotted along with their colocalization status. 1 pixel=0.01 μm^2. *n* indicates the number of nuclei (D) and puncta (E) used in the quantification. The box plots in D and E show the median (line), interquartile range (IQR; box), and 1.5 times the IQR from the first and third quartiles (whiskers). DMSO was used as a vehicle control for all treatments. (F) Snapshots from Movies 1 and 2 showing a nucleus; the dashed line marks the nuclear boundary. mRuby2-fused Coilin was expressed in HeLa cells, and the cells were scanned every 2 min over a 6 h period (divided into 3 h each for harmine treatment and recovery). Rapid localization changes of Coilin were observed in both phases of the experiment. These experiments were repeated at least three times. Time is shown in minutes. Scale bar: 10 μm.

Journal of Cell Science (2024) 137, jcs261834. doi:10.1242/jcs.261834

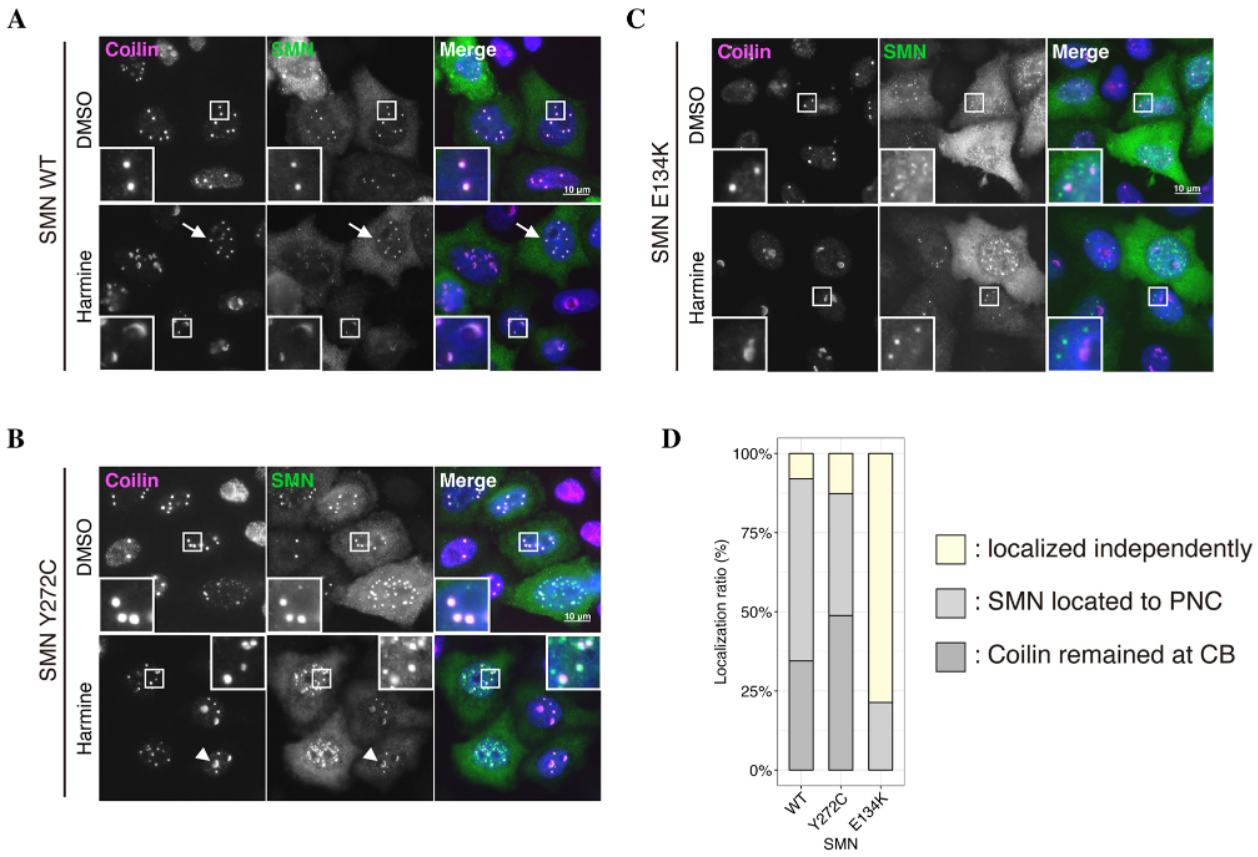

Fig. 6. Detection of cellular interaction between Coilin and overexpressed SMN based on the harmine-induced localization change. (A-C) Wild-type and mutant SMN proteins were expressed in HeLa cells to detect their localization. Mutations introduced into SMN are indicated on the left side of the panels. The top and bottom panels represent cells that were mock treated (DMSO) and treated with harmine (50 µM, 4 h), respectively. Arrows indicate a Cajal body; arrowheads indicate the PNC (detected by anti-Coilin). Corresponding anti-FLAG labels for SMN are also shown. Areas outlined with white squares are shown in the insets. In cells expressing wild-type SMN (SMN WT) (A) and SMN Y272C (B), both the Cajal bodies and PNC contain Coilin and SMN. Although SMN WT often colocalized with Coilin at the PNC and to a lesser extent at Cajal bodies, SMN Y272C predominantly remained at Cajal bodies, colocalizing with Coilin after harmine treatment. The localization of SMN E134K (C) was observed to be independent from Coilin, regardless of harmine treatment. (D) A bar graph shows the localization patterns observed in each SMN WT and mutant variant. Classification of localization patterns and raw counts of cells in each pattern are detailed in Fig. S7. Cell count data were derived from two independent experiments. CB, Cajal body.

Overexpression of SMN Y272C mutant causes the formation of unusual Cajal bodies with mixed distribution with Coilin, in which snRNA is retained

Interestingly, the cells with higher expression of SMN WT formed large cytoplasmic granules (Fig. 7A), but these granules were reduced in the case of SMN Y272C. On the other hand, nuclear foci produced by Y272C overexpression were observed to be larger than those of the wild type. The reduction of cytoplasmic granules in the Y272C mutant may reflect that the Y272C mutant promotes larger nuclear foci, thereby sequestering SMN to the nucleus. As shown in Fig. 7B, quantification of puncta size confirmed that Y272C induced an increase in the size of nuclear foci. This suggests that, although the SMN Y272C mutant lacks multimerization activity, it is still capable of forming large aggregates.

Using super-resolution microscopy, we examined the structural differences between SMN WT- and SMN Y272C-containing Cajal bodies. Although Cajal bodies of normal size showed no difference between SMN WT and Y272C, the enlarged Cajal bodies formed by Y272C expression exhibited an irregular morphology. In larger atypical Cajal bodies, both SMN and Coilin thoroughly coincided in this aberrant, ring-like structure (Fig. 7C). Normally, most mature large Cajal bodies are observed as attached spheres of the separated puncta of SMN and Coilin, with snRNAs colocalized alongside Coilin puncta. In contrast, in the atypical structure caused by the Y272C mutant, the U2 snRNA, which is similar to Coilin, was also not segregated from SMN (Fig. 7D). The aggregate containing SMN Y272C is unable to segregate Coilin and U2 snRNA from SMN, underscoring the essential role of multimerization in their segregation.

Finally, to determine whether the Tudor domain-mediated SMN-Coilin interaction is crucial for the assembly of the atypical Y272C structure, we examined the localization of the SMN E134K/Y272C double mutant upon harmine treatment. Protein expression levels remained relatively constant across mutants after harmine exposure (Fig. S2B), and the response of this double mutant to harmine mirrored that of the E134K mutant (Fig. 8A). Thus, the interaction between SMN and Coilin through the Tudor domain plays a role in the assembly step of the atypical Y272C structure, as well as the typical Cajal bodies.

DISCUSSION

The hypothetical role of SMN multimerization in its dissociation from the Cajal body

Our analysis, aimed at visualizing the fine structure of Cajal bodies by detecting three major components – SMN, Coilin and

Journal of Cell Science (2024) 137, jcs261834. doi:10.1242/jcs.261834

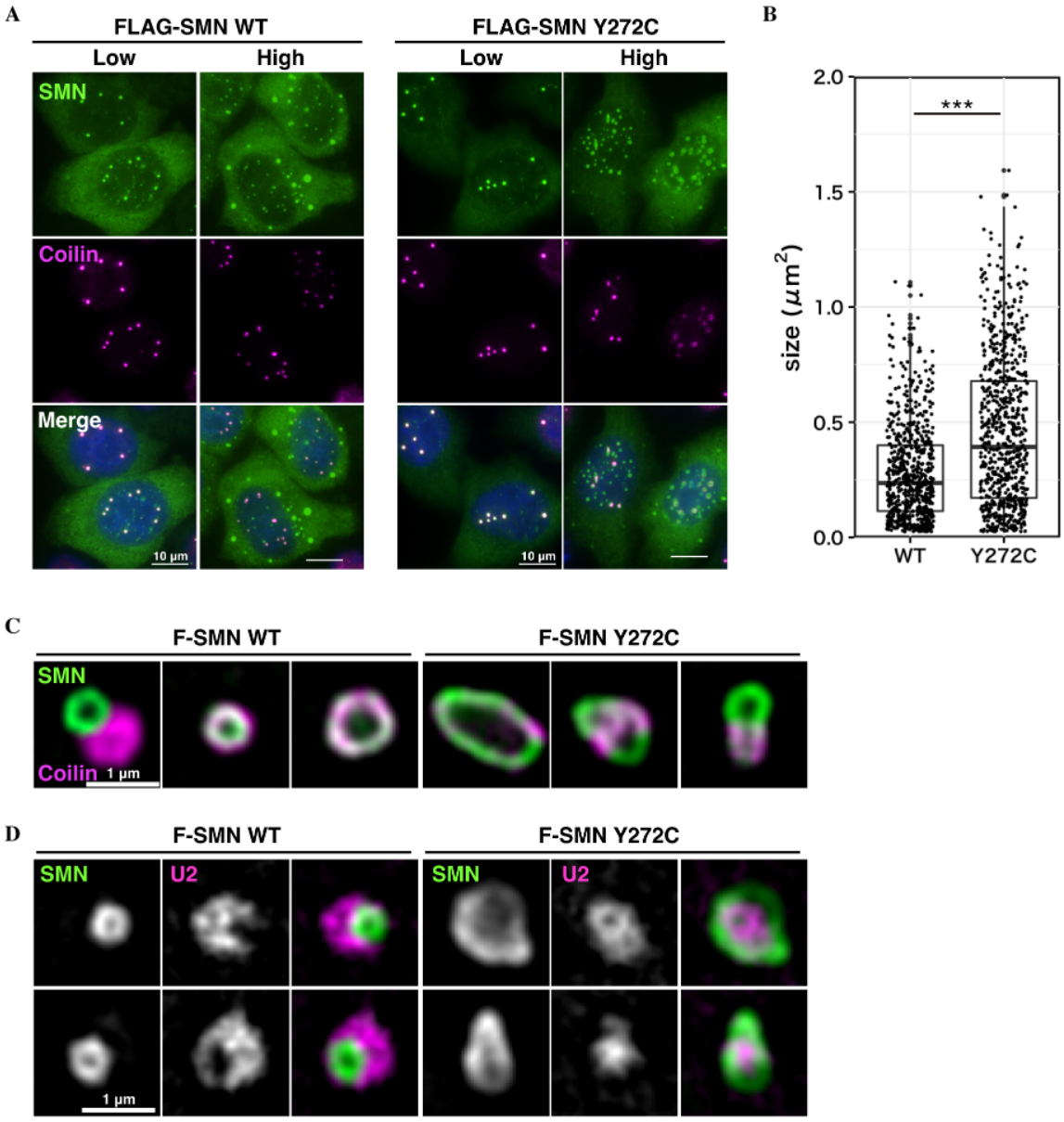

Fig. 7. SMN Y272C induces the formation of larger irregularly shaped Cajal bodies in the nucleus. (A) Localization of overexpressed SMN (anti-FLAG) and endogenous Coilin (anti-Coilin) in HeLa cells. High expression levels of wild-type SMN (SMN WT) lead to the formation of large cytoplasmic granules. In contrast, expression of SMN Y272C results in reduced cytoplasmic granules and enlarged nuclear puncta compared with SMN WT. (B) Comparison of nuclear puncta size between SMN WT- and SMN Y272C-expressing cells. The Wilcoxon rank sum test was used for comparison (***P=4.57×10^{-24}). Puncta sizes were calculated from orthogonal projection images generated from z-stacks acquired by confocal microscopy. The experiments were independently performed three times, and the quantified data from all experiments exhibited a similar trend. One representative plot is displayed (n=86 and 98; number of nuclei used for quantification). The box plot shows the median (line), interquartile range (IQR; box), and 1.5 times the IQR from the first and third quartiles (whiskers). (C) SIM images of Cajal bodies, stained with anti-FLAG for SMN (green) and anti-Coilin (magenta). SMN WT displays distinct puncta or uniform colocalization of SMN and Coilin (left panels). SMN Y272C forms similar structures, but larger Cajal bodies exhibit irregular, pretzel-like shapes with partial Coilin colocalization (right panels). (D) U2 snRNA localization in Cajal bodies observed by super-resolution microscopy (SMN, green; U2, magenta). In SMN Y272C cells, snRNA localizes within the pretzel-like structures (right panels), whereas in SMN WT cells, snRNA puncta are separate from the SMN WT Cajal bodies (left panels). Images in C and D are representative of three and two independent experiments, respectively.

snRNA – revealed that SMN was often positioned separately from Coilin, consistent with previous reports (Courchaine et al., 2021; Hebert et al., 2002; Liu and Dreyfuss, 1996; Young et al., 2001). However, the shape of the SMN puncta varied with size. Smaller SMN bodies appeared granular, whereas larger bodies were observed as rings. These configurations resemble previously reported structures of small nucleolar ribonucleoprotein (snoRNP) in the dense fibrillar component of the nucleolus, interpreted as clustered distributions (Yao et al., 2019). Because no ring structures were observed in live imaging of Cajal bodies and Gems, and, moreover, this ring-like shape is visible under an optical microscope, and z-slices of the bodies at any position observed by SIM showed the ring, we believe that these bodies indeed form a ring. The restricted clustered arrangement of SMN or other components could artificially

Journal of Cell Science (2024) 137, jcs261834. doi:10.1242/jcs.261834

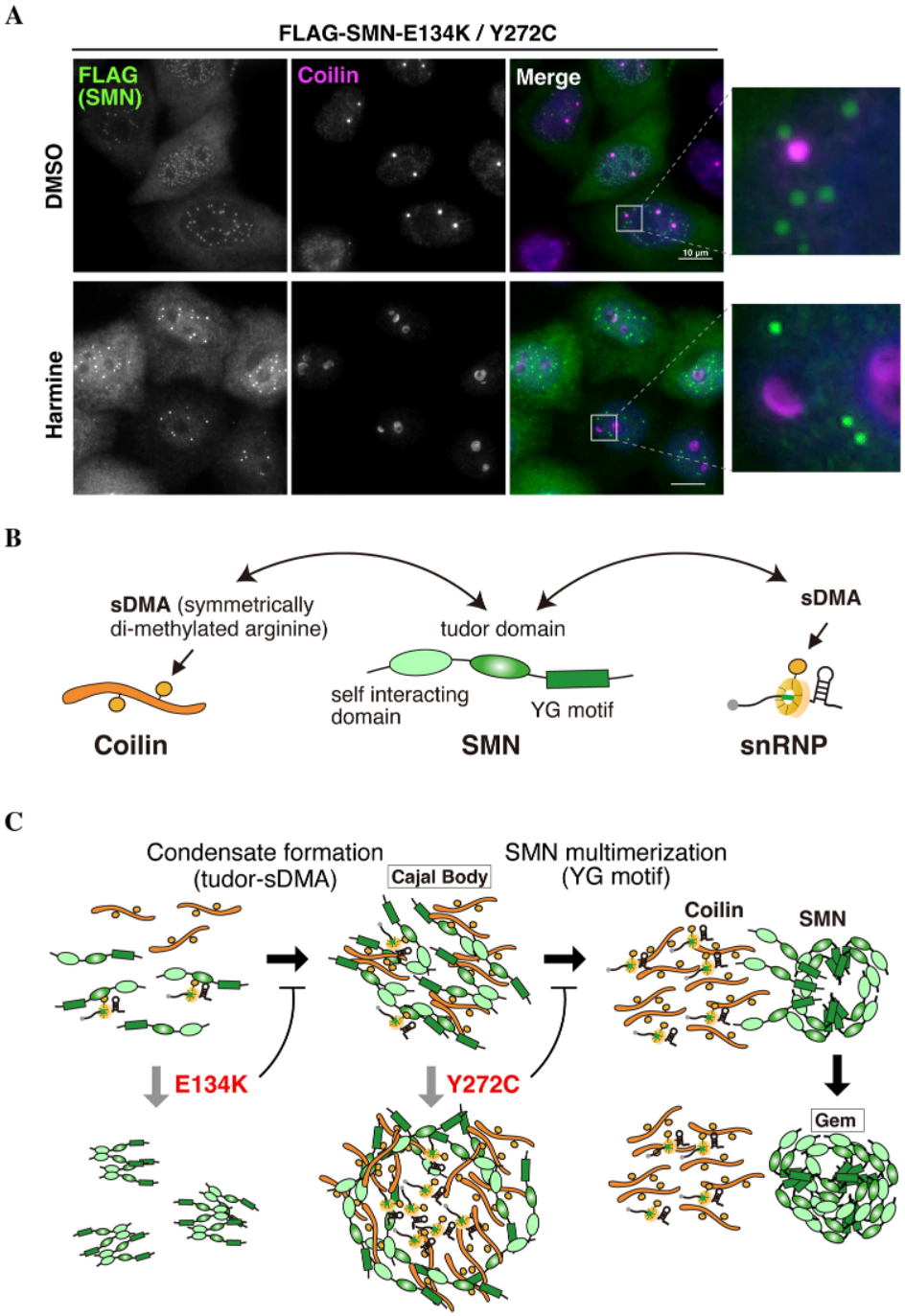

Fig. 8. Deficiency of the SMN E134K/Y272C double mutant in interacting with Coilin. (A) Localization of the SMN E134K/Y272C double mutant (green) in HeLa cells. Similar to SMN E134K alone, this double mutant exhibits a distinct Coilin localization (magenta), independent of harmine treatment (50 µM, 4 h). DMSO was used as a vehicle control. Boxes indicate regions presented as magnified views showing no colocalization between SMN and Coilin, both in the presence and absence of harmine. Images are representative of two independent experiments. (B,C) Schematic illustration of the proposed roles of SMN multimerization in this study. (B) Essential protein domains and motifs for Cajal body formation. The SMN Tudor domain binds symmetrically di-methylated arginine (sDMA) in the RG motif of Coilin and Sm proteins, facilitating Cajal body formation. The YG domain of SMN is involved in multimerization. (C) After nuclear import, SMN interacts with Coilin to form Cajal bodies through multivalent interactions involving the Tudor domain. As Cajal bodies enlarge and the concentration of SMN reaches a threshold for multimerization, the multimerized SMN structure is ejected from the Cajal body, potentially due to conformational changes that disrupt the multivalent Tudor domain interactions. The SMN Y272C mutant, which is impaired in multimerization, fails to detach from Coilin puncta, leading to the formation of larger, irregularly shaped nuclear bodies. This could result in delayed nuclear export of SMN, affecting the recycling process of SMN.

result in the formation of this ring. For example, the restricted structure may hinder antibody access to the core or, alternatively, it may resist fixation, causing the proteins to fall out of the core. Although the ring-like shape of SMN puncta might be an artifact of immunolabeling, its clear distinction from Coilin puncta suggests it could reflect a restricted arrangement of components.

The ring-like shape observed within larger bodies leads us to speculate that an increased concentration of SMN triggers its multimerization via the YG motif, resulting in such structures. Observations indicate that the inclusion of SMN Y272C, a multimerization-defective mutant, causes a disturbance in the separation of SMN and Coilin, resulting in the formation of larger bodies, supporting this hypothesis. Furthermore, in normally separated Cajal bodies, snRNAs were found to overlap entirely with Coilin, but not with SMN. This suggests that the separation of SMN as a ring-like structure could be associated with the release of snRNPs. As illustrated in Fig. 8B, SMN binds both Coilin and Sm proteins in snRNP via the Tudor domain, and the C-terminal domain of SMN has been demonstrated to bind SmB protein (encoded by *SNRPB*) (Liu et al., 1997). Consequently, YG motif-dependent multimerization might also play a role in facilitating the release of snRNPs into the Coilin condensate. Determining whether the conformation of SMN in the ring-like structure restricts the interaction surface to Coilin and snRNPs would be interesting.

Possible mechanisms of harmine-induced PNC translocation of Coilin

We have discovered that harmine, a β-carboline alkaloid derived from *Peganum harmala*, serves as an effective tool for chemically dissecting Cajal bodies. Harmine is reported to round nucleoli (Seegers et al., 1985), a phenomenon commonly observed with small compounds that disrupt ribosomal RNA (rRNA) processing (Burger et al., 2010). Significantly, harmine can intercalate into double-stranded DNA, inhibiting topoisomerase *in vitro* (Cao et al., 2005; Duportail and Lami, 1975; Herraiz et al., 2010; Sobhani et al., 2002). Thus, harmine might impede rRNA processing either by obstructing RNA polymerase I or by inhibiting topoisomerase I and other processing factors. The inhibition of rRNA processing leads to structural changes in nucleoli (Lafontaine et al., 2021), potentially triggering the redistribution of nucleolar proteins that bind to Coilin, such as Nopp140 and fibrillarin. Camptothecin, another topoisomerase I inhibitor that also inhibits rRNA processing (Burger et al., 2010), demonstrated similar effects to harmine in our study, supporting this hypothesis. Testing with harmine analogs revealed that harmine is more effective than others, possibly owing to structural features that are essential for disrupting rRNA processing. However, harmol has been shown to exhibit a similar spectrum of inhibitory activities to harmine against several kinases (Tarpley et al., 2021), suggesting that their structural and chemical properties may be relatively close, especially when compared with harmane and harmaline. Additionally, a comparison of the DNA-binding affinities of β-carboline alkaloids revealed higher affinity values for harmine and harmol than for harmane and harmaline, with harmine displaying greater affinity than harmol (Taira et al., 1997). The fact that the order of DNA-binding affinities corresponds with their ability to induce the PNC translocation of Coilin supports the hypothesis that harmine induces nucleolar stress by binding to nucleolar rDNA and abrogating rRNA production. The precise step of rRNA processing affected by harmine is still unclear, and alternative mechanisms might exist, such as harmine directly inducing the emergence of Coilin-binding proteins on the PNC surface, thereby causing the translocation of Coilin to PNC. Another possibility is that the damage triggered by harmine and other PNC translocation-inducing compounds disturbs the cell cycle, which indirectly alters the distribution of Coilin as Cajal body formation is regulated by the cell cycle. In addition, harmine may also cause the transcriptional arrest of U2 snRNA, which could explain the disappearance of Coilin from Cajal bodies.

A prominent feature of harmine as a tool compound is its reversible action. Actinomycin D induced similar coilin localization at even in lower concentrations (0.05 µg/ml), in which transcriptional inhibition occurs only for class 1 genes (Bensaude, 2011); however, the effect was irreversible. Although the precise mechanism by which harmine induces the Coilin localization is unknown, the dynamics of Coilin entering and exiting PNC were remarkably rapid. It is uncertain whether the re-assembly of Cajal bodies after harmine removal accurately reflects the normal assembly process, considering the actions of harmine in expelling Coilin from these bodies. Furthermore, newly formed Cajal bodies likely differ in both position and number compared with those before harmine treatment, which were smaller but more numerous. This may reflect that the formation process of condensates in the recovery phases occurs based on relatively simple molecular interactions of protein components. These interactions may not include those with snRNA and its transcription, or the genomic domains that normally contribute to the cell cycle-dependent formation of Cajal bodies.

Nevertheless, the observation that Gem-like structures did not consistently recruit Coilin from the Cajal body might suggest that Gem serves as a recycling place for SMN and the Gemin complex (Morris, 2008). Yet it is puzzling why SMN in Gem-like structures does not effectively recruit Coilin, despite its abundance. As discussed above, determining whether the conformation of SMN in the ring-like structure limits its interaction with Coilin would also help to resolve this issue.

Analysis of the molecular behavior of SMN mutants using harmine as a tool compound

We have also demonstrated that harmine is an effective tool for visualizing cellular interactions between SMN and Coilin, as indicated by their synchronized localization change upon harmine treatment. It was challenging to visually identify a potential defect in the Coilin binding of the SMN E134K mutant within a cellular context. This difficulty arises because the SMN E134K mutant forms numerous small nuclear dots and these dots often appear adjacent to Coilin. However, the SMN E134K mutant protein fails to co-migrate with Coilin after harmine treatment, clearly suggesting a lack of interaction with Coilin. In contrast, the SMN Y272C mutant, which lacks multimerization activity, leads to the formation of large irregularly shaped nuclear bodies. Although this finding deviates from previous research (Hua and Zhou, 2004), the use of GFP fusion proteins in the earlier study might explain this inconsistency. Both the SMN E134K and Y272C mutants were unable to facilitate Sm core assembly on U1 snRNA (Shpargel and Matera, 2005), which is consistent with the observation that neither mutant forms canonical Cajal bodies. Compared with the wild-type protein, the Y272C mutant exhibited reduced cytoplasmic granules and enlarged nuclear bodies. Furthermore, harmine treatment in cells expressing this mutant resulted in the sequestration of Coilin within these nuclear bodies, suggesting that the Y272C mutation impairs the dissociation of SMN from Coilin, further strengthening the crucial role of multimerization in SMN release from the Cajal body, as illustrated in Fig. 8C. A previous study showed that E134K, which lacks the ability to bind Importin β, is defective in nuclear import, and Y272C, despite its ability to bind Importin β, is similarly defective in nuclear import (Narayanan et al., 2004). Our findings suggest that SMN multimerization plays multiple roles in its shuttling, potentially explaining the severe disease caused by this mutant. Analyzing other SMN mutants with reduced multimerization activity, similar to Y272C, could further corroborate this model. In our study, these experiments were carried out in the presence of endogenous wild-type proteins. The absence of the wild-type protein might significantly alter the aggregates formed by the SMN Y272C and E134K mutant. Obviously, further studies are needed to explore these possibilities and to confirm the role of multimerization in SMN recycling.

MATERIALS AND METHODS

Cell culture and reagents

HeLa, HCT116 and U2OS cells were maintained in DMEM with 10% FBS, while HepG2 cells were maintained in high-glucose DMEM with 10% FBS. Small compounds used in this study were purchased, except for the compounds library. Chemical compound library and hit compounds were provided by the Drug Discovery Initiative (The University of Tokyo, Japan). Harmine, harmaline (Sigma, 286044 and 51330, respectively), harmane (WAKO, 328-40031), harmol (TCI, H1360) and INDY (Sigma, SML1011) were purchased from manufacturers, as indicated. Expression vectors for Coilin, SMN and the SMN mutants were made by inserting the desired open reading frame into T2KXIG plasmids (Kawakami et al., 2004) encoding each tag sequence using a Gibson assembly kit (NEB, E2611 or E2621). Mutated SMN clones were produced by PCR using the following primers: SMN_E134K_s, 5′-GGAAATAGAAAGGAGCAAAATCTGTCCGAT-3′;

SMN_E134K_as, 5′-TTGCTCCTTTCTATTTCCATATCCAGTGTAAA-3′; SMN_Y272C_s1, 5′-GAGTGGCTGTCATACTGGCTATTATATGGGTTT-3′; and SMN_Y272C_as1, 5′-CAGTATGACAGCCACTCATGTACCAT-GAA-3′. Vector maps and sequences confirmed by Sanger sequencing have been deposited in Figshare (https://doi.org/10.6084/m9.figshare.26048449). Antibodies used in this study are listed in Table S1.

Western blotting

To detect Coilin and SMN after compound treatment, cells were washed with PBS and collected with 2× SDS-PAGE sample buffer [100 mM Tris-HCl (pH 6.8), 4% SDS, 20% glycerol, 0.01% bromophenol blue and 10% 2-mercaptoethanol]. Cell extracts were heated at 95°C for 5 min and sonicated. A 12.5% polyacrylamide gel was used to separate cell extracts by SDS-PAGE, followed by transfer to a PVDF membrane using a semi-dry blotter. A membrane was reacted with the primary antibody for 1 h at room temperature after blocking with 2.5% skim milk in PBST (PBS, 0.01% Tween-20) for 20 min. After three washes with PBST, the secondary antibody reaction was performed for 1 h at room temperature. Secondary antibodies were labeled with Alexa Fluor 680 (Molecular Probes) or IRDye 800 (Rockland) and used at a 6000-fold dilution in PBST. After three washes with PBST, signals were detected using Odyssey (Infrared Imaging System, LI-COR Biosciences).

Immunofluorescence

HeLa cells were cultured in six-well plates where coverslips were placed. Cells were fixed in 4% paraformaldehyde for 5 min after treatment of compounds at the indicated times. Fixed cells were further treated with 0.5% Triton-X100 in PBS(−) for 5 min to permeabilize the cell membrane before reacting with the antibody. Antibodies were diluted to 1:200 by PBS(−) supplemented with 0.1% FBS. Diluted antibodies reacted with the cells on the coverslip for 1 h at 37°C. To detect the primary antibodies, Alexa488/Rhodamine/Cy3-labeled anti-mouse/rabbit IgG antibodies were used as second antibodies. After washing and mounting the cover glass, cells were observed by BZ-8000 (KEYENCE) or IX70 mounted with DP72 (Olympus). The brightness and contrast of the obtained images were adjusted using the window/level function of ImageJ with the same parameters of window level and width within each set of experiments.

Confocal microscopy

Images were acquired with an LSM900 (ZEISS) using a 60× objective (NA1.20) with 11 *z*-stacks of 400 nm at 4 µm intervals. After image acquisition, Airyscan Processing was applied to the images, and the maximum intensity was obtained by orthogonal projection to the *xy* plane using ZEN 3.4 software.

Super-resolution microscopy

Cells were incubated in a dish containing a cover glass (Assistent 18 mm Deckglas-Diche 0.17±0.01 mm) coated with 0.1 mg/ml poly-L-lysine (Sigma), followed by 4% paraformaldehyde (PFA)/HCMF fixing solution and fixed at room temperature for 5 min. After washing three times with HCMF, 0.5% TritonX-100/PBS was added and permeabilized for 5 min. After three washes with TBS, a secondary antibody reaction with a pair of fluorescently labeled antibodies (anti-RbIgG-Cy2/anti-MsIgG-Cy3 or anti-RbIgG-Cy3/anti-MsIgG-Cy2) was performed at 37°C for 1 h. After three washes with TBS, TDE was replaced with 10%, 25%, 50% and 97% TDE (all in 0.01× PBS) for 5 min at room temperature. After replacement, cells were mounted with TDE mounting agent (97% TDE, 2% Dabco, 0.1 µg/ml DAPI and 0.01× PBS). Fifty *z* stacks were taken at 100 nm intervals with a 100× objective (NA 1.46; ZEISS) using an ELYRA PS1 (Zeiss). SIM images were acquired using ZEN 2011 software with default parameter settings. Channel alignment was performed using an alignment file. The data presented in the figures were taken from a single image in the *z* stacks where the structure appeared largest.

Live imaging

Cells cultured in a glass-bottom dish were replaced with Phenol Red-free medium immediately before live imaging. The dish was placed in a chamber at 37°C and 5% CO_2, and 11 *z*-stacks of 400 nm were taken at 400 nm interval with a 60× objective (NA1.20) using LSM900 (ZEISS) at a 2 min interval. harmine was added and removed with the lid of the chamber open, without moving the dish, using a pipette. After image acquisition, Airyscan Processing was applied to the images, and the maximum intensity was obtained by orthogonal projection to the *xy* plane using ZEN 3.4 software.

snRNA FISH

Probe preparation

Human U2 snRNA and other RNA was cloned into pGEM-T-Easy and the insertion direction and sequence were verified by Sanger sequencing. To prepare the template DNA fragment for *in vitro* transcription, a cassette of the promoter and insert cDNA was amplified by PCR with the M13 primer pair using the plasmid as a template. The amplified DNA fragment was purified and used for *in vitro* transcription using the DIG/FITC RNA labeling kit (Roche). Transcribed RNA was purified using CENTRISEP Spin Column (PRINCETON SEPARATIONS). The RNA probe was mixed with an equal volume of formamide and sored at −20°C.

Fixation and hybridization

Cells cultured in a dish with cover glass (Assistent 18 mm Deckglas-Diche 0.17±0.01 mm) coated with 0.1 mg/ml poly-L-lysine (Sigma) were fixed with 4% PFA/HCMF at room temperature for 10 min. The cells were then washed with PBS and permeabilized with 0.5% TritonX-100/PBS for 10 min. Fixed samples were soaked in prehybridization solution [50% formamide, Denhardt's solution (2×SSC, 1.5 mM trisodium citrate and 15 mM NaCl), 10 mM EDTA and 100 µg/ml yeast tRNA, 0.01%] at 55°C for 2 h. After removal of prehybridization solution, samples were reacted with RNA probe diluted 100-fold with hybridization solution (prehybridization solution plus 5% dextran sulfate) in a humidified container at 50°C overnight.

Wash and mount

After hybridization, samples were washed twice with 50% formamide and 2×SSC at 50°C for 30 min. The cells were then rinsed with RNase buffer [10 mM Tris-HCl (pH 8.0), 500 mM NaCl, 1 mM EDTA and 0.01% Tween-20] and treated with RNase A (10 µg/ml RNaseA, RNaseA buffer) at 37°C for 1 h. After rinsing with RNase buffer again, the samples were washed with 2×SSC solution and 0.2×SSC solution (0.2×SSC and 0.01% Tween-20) at 50°C for 30 min each and transferred to TBST (TBS, 0.01% Tween-20). Samples were soaked in Blocking Regent (Roche) dissolved in TBST for 10 min at room temperature. After three washes with TBST, the primary antibody was reacted a pair of fluorescent label antibodies (anti-RbIgG-Cy2/anti-MsIgG-Cy3 or anti-RbIgG-Cy3/anti-MsIgG-Cy2) for 1 h at room temperature, and then the antibody was fixed in 4% PFA/HCMF for 10 min at room temperature after two washes with TBST and one wash with PBS. After fixation, the cells were washed once with PBS, twice with TBST and once with deionized water. Coverslips were mounted with PVA mounting agent.

Image quantification and statistical analysis

Cell profiler (version 3.1.9) was used to quantify the size and number of Cajal bodies from images. This pipeline includes a module to exclude the cells that are too bright or too dark compared with the average brightness. As average brightness varied among experiments, parameters were adjusted for each data although the order of modules in the pipeline was not changed. For further analysis, Cell profiler (version 4.2.6) was used. To analyze overlapping of two objects identified by double-stained images, a threshold was set at 10 pixels between the centers of both objects. For identifying objects, a threshold was set to recognize those larger than 5 pixels. To calculate the colocalization coefficient values, the Pearson correlation coefficient (PCC) was used for proteins that are primarily localized in nuclear dots recognized as Cajal bodies or Gems. Conversely, when the target protein was localized in two places, such as nucleoli and Cajal bodies, as observed for Nopp140, Manders' overlap coefficient (MOC), using the auto-threshold method developed by Costes, was used to analyze colocalization with another protein. These pipelines designed for quantitative analysis are available upon request. Analyzed data from Cell

profiler was exported as an SQLite database and then imported into R for further statistical analysis and visualization. To draw Venn diagrams, the eulerr package (https://rdrr.io/cran/eulerr/) was used to obtain parameters, and the Venn diagrams were subsequently produced using ggplot2 based on these parameters. For the statistical analysis, the Wilcoxon rank sum test was used to calculate the *P*-value using R.

Acknowledgements
We thank Rie Nakaido, Yumi Komatsu, and the staff of the Center for Research and Education on Drug Discovery (Hokkaido University) for their assistance with administrative procedures and chemical and lab management. We also thank Drs Tetsuro Hirose, Soichiro Kawagoe, Hiroyuki Kumeta and Tomohide Saio, and lab members for valuable discussion.

Competing interests
The authors declare no competing or financial interests.

Author contributions
Conceptualization: H.M.; Investigation: S.O., A.F., D.K., R.Y., H.M.; Resources: R.Y., S.N., H.M.; Data curation: S.O., H.M.; Writing - original draft: S.O., H.M.; Writing - review & editing: S.N., H.M.; Visualization: S.O., H.M.; Supervision: S.N., H.M.; Project administration: S.N., H.M.; Funding acquisition: S.N., H.M.

Funding
This study was supported by the Japan Science and Technology Agency Support for Pioneering Research Initiated by the Next Generation (JPMJSP2119 to S.O.) and the Japan Society for the Promotion of Science (KAKENHI 16K08225, 20H04687, 20K07028 and 23K06093 to H.M., and KAKENHI Grant-in-Aid for Transformative Research Areas 21H05274 to S.N.). This study was also supported by the Platform Project for Supporting Drug Discovery and Life Science Research [Basis for Supporting Innovative Drug Discovery and Life Science Research (BINDS)] from the Japan Agency for Medical Research and Development (JP21am0101001).

Data availability
Vector maps and sequences confirmed by Sanger sequencing have been deposited in Figshare (https://doi.org/10.6084/m9.figshare.26048449). All other relevant data can be found within the article and its supplementary information.

Peer review history
The peer review history is available online at https://journals.biologists.com/jcs/lookup/doi/10.1242/jcs.261834.reviewer-comments.pdf

Reference
Bain, J., Plater, L., Elliott, M., Shpiro, N., Hastie, C. J., McLauchlan, H., Klevernic, I., Arthur, J. S. C., Alessi, D. R. and Cohen, P. (2007). The selectivity of protein kinase inhibitors: a further update. *Biochem. J.* **408**, 297-315. doi:10.1042/BJ20070797

Bensaude, O. (2011). Inhibiting eukaryotic transcription: Which compound to choose? How to evaluate its activity?: Which compound to choose? How to evaluate its activity? *Transcription* **2**, 103-108. doi:10.4161/trns.2.3.16172

Bohmann, K., Ferreira, J. A. and Lamond, A. I. (1995). Mutational analysis of p80 coilin indicates a functional interaction between coiled bodies and the nucleolus. *J. Cell Biol.* **131**, 817-831. doi:10.1083/jcb.131.4.817

Borcherds, W., Bremer, A., Borgia, M. B. and Mittag, T. (2021). How do intrinsically disordered protein regions encode a driving force for liquid–liquid phase separation? *Curr. Opin. Struct. Biol.* **67**, 41-50. doi:10.1016/j.sbi.2020.09.004

Burger, K., Mühl, B., Harasim, T., Rohrmoser, M., Malamoussi, A., Orban, M., Kellner, M., Gruber-Eber, A., Kremmer, E., Hölzel, M. et al. (2010). Chemotherapeutic drugs inhibit ribosome biogenesis at various levels. *J. Biol. Chem.* **285**, 12416-12425. doi:10.1074/jbc.M109.074211

Butchbach, M. E. R. (2021). Genomic variability in the survival motor neuron genes (SMN1 and SMN2): implications for spinal muscular atrophy phenotype and therapeutics development. *Int. J. Mol. Sci.* **22**, 7896. doi:10.3390/ijms22157896

Cao, R., Peng, W., Chen, H., Ma, Y., Liu, X., Hou, X., Guan, H. and Xu, A. (2005). DNA binding properties of 9-substituted harmine derivatives. *Biochem. Biophys. Res. Commun.* **338**, 1557-1563. doi:10.1016/j.bbrc.2005.10.121

Carmo-Fonseca, M., Pepperkok, R., Carvalho, M. T. and Lamond, A. I. (1992). Transcription-dependent colocalization of the U1, U2, U4/U6, and U5 snRNPs in coiled bodies. *J. Cell Biol.* **117**, 1-14. doi:10.1083/jcb.117.1.1

Courchaine, E. M., Barentine, A. E. S., Straube, K., Lee, D.-R., Bewersdorf, J. and Neugebauer, K. M. (2021). DMA-tudor interaction modules control the specificity of in vivo condensates. *Cell* **184**, 3612-3625.e17. doi:10.1016/j.cell.2021.05.008

Dundr, M., Hebert, M. D., Karpova, T. S., Stanek, D., Xu, H., Shpargel, K. B., Meier, U. T., Neugebauer, K. M., Matera, A. G. and Misteli, T. (2004). In vivo kinetics of Cajal body components. *J. Cell Biol.* **164**, 831-842. doi:10.1083/jcb.200311121

Duportail, G. and Lami, H. (1975). Studies of the interaction of the fluorophores harmine and harmaline with calf thymus DNA. *Biochim. Biophys. Acta* **402**, 20-30. doi:10.1016/0005-2787(75)90365-2

Göckler, N., Jofre, G., Papadopoulos, C., Soppa, U., Tejedor, F. J. and Becker, W. (2009). Harmine specifically inhibits protein kinase DYRK1A and interferes with neurite formation. *FEBS J.* **276**, 6324-6337. doi:10.1111/j.1742-4658.2009.07346.x

Handwerger, K. E., Murphy, C. and Gall, J. G. (2003). Steady-state dynamics of Cajal body components in the Xenopus germinal vesicle. *J. Cell Biol.* **160**, 495-504. doi:10.1083/jcb.200212024

Hebert, M. D., Szymczyk, P. W., Shpargel, K. B. and Matera, A. G. (2001). Coilin forms the bridge between Cajal bodies and SMN, the spinal muscular atrophy protein. *Genes Dev.* **15**, 2720-2729. doi:10.1101/gad.908401

Hebert, M. D., Shpargel, K. B., Ospina, J. K., Tucker, K. E. and Matera, A. G. (2002). Coilin methylation regulates nuclear body formation. *Dev. Cell* **3**, 329-337. doi:10.1016/S1534-5807(02)00222-8

Herraiz, T., González, D., Ancín-Azpilicueta, C., Arán, V. J. and Guillén, H. (2010). β-Carboline alkaloids in Peganum harmala and inhibition of human monoamine oxidase (MAO). *Food Chem. Toxicol.* **48**, 839-845. doi:10.1016/j.fct.2009.12.019

Hirose, T., Ninomiya, K., Nakagawa, S. and Yamazaki, T. (2022). A guide to membraneless organelles and their various roles in gene regulation. *Nat. Rev. Mol. Cell Biol.* **24**, 288-304. doi:10.1038/s41580-022-00558-8

Hua, Y. and Zhou, J. (2004). Modulation of SMN nuclear foci and cytoplasmic localization by its C-terminus. *Cell. Mol. Life. Sci.* **61**, 2658-2663. doi:10.1007/s00018-004-4300-z

Kawakami, K., Takeda, H., Kawakami, N., Kobayashi, M., Matsuda, N. and Mishina, M. (2004). A transposon-mediated gene trap approach identifies developmentally regulated genes in zebrafish. *Dev. Cell* **7**, 133-144. doi:10.1016/j.devcel.2004.06.005

Kii, I., Sumida, Y., Goto, T., Sonamoto, R., Okuno, Y., Yoshida, S., Kato-Sumida, T., Koike, Y., Abe, M., Nonaka, Y. et al. (2016). Selective inhibition of the kinase DYRK1A by targeting its folding process. *Nat. Commun.* **7**, 1-14.

Kim, H., Sablin, S. O. and Ramsay, R. R. (1997). Inhibition of monoamine oxidase A by beta-carboline derivatives. *Arch. Biochem. Biophys.* **337**, 137-142. doi:10.1006/abbi.1996.9771

Lafontaine, D. L. J., Riback, J. A., Bascetin, R. and Brangwynne, C. P. (2021). The nucleolus as a multiphase liquid condensate. *Nat. Rev. Mol. Cell Biol.* **22**, 165-182. doi:10.1038/s41580-020-0272-6

Liu, Q. and Dreyfuss, G. (1996). A novel nuclear structure containing the survival of motor neurons protein. *EMBO J.* **15**, 3555-3565. doi:10.1002/j.1460-2075.1996.tb00725.x

Liu, Q., Fischer, U., Wang, F. and Dreyfuss, G. (1997). The spinal muscular atrophy disease gene product, SMN, and its associated protein SIP1 are in a complex with spliceosomal snRNP proteins. *Cell* **90**, 1013-1021. doi:10.1016/S0092-8674(00)80367-0

Martin, R., Gupta, K., Ninan, N. S., Perry, K. and Van Duyne, G. D. (2012). The survival motor neuron protein forms soluble glycine zipper oligomers. *Structure* **20**, 1929-1939. doi:10.1016/j.str.2012.08.024

Matera, A. G. (1998). Of coiled bodies, gems, and salmon. *J. Cell. Biochem.* **70**, 181-192. doi:10.1002/(SICI)1097-4644(19980801)70:2<181::AID-JCB4>3.0.CO;2-K

Meier, U. T. (2017). RNA modification in Cajal bodies. *RNA Biol.* **14**, 693-700. doi:10.1080/15476286.2016.1249091

Morris, G. E. (2008). The Cajal body. *Biochim. Biophys. Acta* **1783**, 2108-2115. doi:10.1016/j.bbamcr.2008.07.016

Narayanan, U., Achsel, T., Lührmann, R. and Matera, A. G. (2004). Coupled in vitro import of U snRNPs and SMN, the spinal muscular atrophy protein. *Mol. Cell* **16**, 223-234. doi:10.1016/j.molcel.2004.09.024

Novotný, I., Malinová, A., Stejskalová, E., Matějů, D., Klimešová, K., Roithová, A., Švéda, M., Knejzlík, Z. and Staněk, D. (2015). SART3-Dependent accumulation of incomplete spliceosomal snRNPs in cajal bodies. *Cell Rep.* **10**, 429-440. doi:10.1016/j.celrep.2014.12.030

Paushkin, S., Gubitz, A. K., Massenet, S. and Dreyfuss, G. (2002). The SMN complex, an assemblyosome of ribonucleoproteins. *Curr. Opin. Cell Biol.* **14**, 305-312. doi:10.1016/S0955-0674(02)00332-0

Pellizzoni, L., Kataoka, N., Charroux, B. and Dreyfuss, G. (1998). A novel function for SMN, the spinal muscular atrophy disease gene product, in pre-mRNA splicing. *Cell* **95**, 615-624. doi:10.1016/S0092-8674(00)81632-3

Rommelspacher, H., May, T. and Salewski, B. (1994). Harman (1-methyl-beta-carboline) is a natural inhibitor of monoamine oxidase type A in rats. *Eur. J. Pharmacol.* **252**, 51-59. doi:10.1016/0014-2999(94)90574-6

Sato, S., Ariga, H. and Maita, H. (2023). Development of a cell-based assay using a split-luciferase reporter for compound screening. *Biol. Pharm. Bull.* **46**, 1010-1014. doi:10.1248/bpb.b23-00042

Seegers, J. C., Ochs, R. L. and Joubert, W. S. (1985). The effect of harmine on the localization of the nucleolar proteins C23 and B23. *Eur. J. Cell Biol.* **37**, 213-215.

Shav-Tal, Y., Blechman, J., Darzacq, X., Montagna, C., Dye, B. T., Patton, J. G., Singer, R. H. and Zipori, D. (2005). Dynamic sorting of nuclear components into distinct nucleolar caps during transcriptional inhibition. *Mol. Biol. Cell* **16**, 2395-2413. doi:10.1091/mbc.e04-11-0992

Shpargel, K. B. and Matera, A. G. (2005). Gemin proteins are required for efficient assembly of Sm-class ribonucleoproteins. *Proc. Natl. Acad. Sci. U. S. A* **102**, 17372-17377. doi:10.1073/pnas.0508947102

Sobhani, A. M., Ebrahimi, S.-A. and Mahmoudian, M. (2002). An in vitro evaluation of human DNA topoisomerase I inhibition by Peganum harmala L. seeds extract and its beta-carboline alkaloids. *J. Pharm. Pharm. Sci.* **5**, 19-23.

Staněk, D. (2017). Cajal bodies and snRNPs - friends with benefits. *RNA Biol.* **14**, 671-679. doi:10.1080/15476286.2016.1231359

Taira, Z., Kanzawa, S., Dohara, C., Ishida, S., Matsumoto, M. and Sakiya, Y. (1997). Intercalation of six. BETA.-carboline derivatives into DNA. *Jap. J. Toxicol. Environ. Health* **43**, 83-91. doi:10.1248/jhs1956.43.83

Tapia, O., Lafarga, V., Bengoechea, R., Palanca, A., Lafarga, M. and Berciano, M. T. (2014). The SMN Tudor SIM-like domain is key to SmD1 and coilin interactions and to Cajal body biogenesis. *J. Cell Sci.* **127**, 939-946.

Tarpley, M., Oladapo, H. O., Strepay, D., Caligan, T. B., Chdid, L., Shehata, H., Roques, J. R., Thomas, R., Laudeman, C. P., Onyenwoke, R. U. et al. (2021). Identification of harmine and β-carboline analogs from a high-throughput screen of an approved drug collection; profiling as differential inhibitors of DYRK1A and monoamine oxidase A and for in vitro and in vivo anti-cancer studies. *Eur. J. Pharm. Sci.* **162**, 105821. doi:10.1016/j.ejps.2021.105821

Uversky, V. N. (2017). Intrinsically disordered proteins in overcrowded milieu: membrane-less organelles, phase separation, and intrinsic disorder. *Curr. Opin. Struct. Biol.* **44**, 18-30. doi:10.1016/j.sbi.2016.10.015

Wang, P., Alvarez-Perez, J.-C., Felsenfeld, D. P., Liu, H., Sivendran, S., Bender, A., Kumar, A., Sanchez, R., Scott, D. K., Garcia-Ocaña, A. et al. (2015). A high-throughput chemical screen reveals that harmine-mediated inhibition of DYRK1A increases human pancreatic beta cell replication. *Nat. Med.* **21**, 383-388. doi:10.1038/nm.3820

Yao, R.-W., Xu, G., Wang, Y., Shan, L., Luan, P.-F., Wang, Y., Wu, M., Yang, L.-Z., Xing, Y.-H., Yang, L. et al. (2019). Nascent Pre-rRNA sorting via phase separation drives the assembly of dense Fibrillar components in the human nucleolus. *Mol. Cell* **76**, 767-783.e11. doi:10.1016/j.molcel.2019.08.014

Young, P. J., Le, T. T., Dunckley, M., Nguyen, T. M., Burghes, A. H. and Morris, G. E. (2001). Nuclear gems and Cajal (coiled) bodies in fetal tissues: nucleolar distribution of the spinal muscular atrophy protein, SMN. *Exp. Cell Res.* **265**, 252-261. doi:10.1006/excr.2001.5186

Yung, B. Y.-M., Bor, A. M.-S. and Chan, P.-K. (1990). Short exposure to actinomycin D induces "Reversible" translocation of protein B23 as well as "reversible" inhibition of cell growth and RNA synthesis in HeLa cells1. *Cancer Res.* **50**, 5987-5991.

Zhu, L. and Brangwynne, C. P. (2015). Nuclear bodies: the emerging biophysics of nucleoplasmic phases. *Curr. Opin. Cell Biol.* **34**, 23-30. doi:10.1016/j.ceb.2015.04.003